CI, CO and 790 m continuum observations of the Orion molecular cloud and ionisation bar

Astron. Astrophys. 299, 179–192 (1995)

ASTRONOMY
AND
ASTROPHYSICS

C I, CO and 790 μm continuum observations of the Orion molecular cloud and ionisation bar

Glenn J. White[1] **and Goeran Sandell**[2]

[1] Department of Physics, Queen Mary and Westfield College, University of London, Mile End Road, London E1 4NS, England
[2] Joint Astronomy Centre, 665 N A'ohoku Place, University Park, Hilo, Hawaii 96720, USA

Received 8 July 1994 / Accepted 22 November 1994

Abstract. The spatial distributions of the $^3P_1 - ^3P_0$ atomic fine structure of carbon (CI), the CO $J = 4 - 3$, the CO $J = 2 - 1$ transitions of CO, ^{13}CO, C^{18}O and C^{17}O and the 790 μm continuum emission have been mapped towards the central region of the Orion molecular cloud (OMC1 cloud), and the Bright Bar ionisation front. The CO data are analysed in a consistent way, allowing the inter isotopomeric abundance ratios to be studied over a wide range of extinction values. The ^{13}CO lines are optically thick; the ^{13}CO abundance being enhanced because of strong isotopic fractionation near the Bright Bar, but less convincingly in the OMC1 cloud. The fractionation occurs mostly in the less opaque regions where the ^{13}CO column density N(^{13}CO) may be enhanced by up to one order of magnitude, relative to the more shielded parts. No isotope selective enhancement of the other CO isotopomers was seen; C^{18}O may in fact show a slight depletion in more exposed material. The C^{18}O and C^{17}O lines are optically thin, and correlated with the 790 μm dust continuum emission. The CI emission comes from hot optically thin gas; the abundance ratios of [CI]/[CO] are typically 0.05 - 0.3, with the larger ratios towards the northern section of the Orion ridge. The CI abundance ratios remain high along the edge of the Bright Bar which is adjacent to the HII region (and the Trapezium cluster which excites it), but decrease in the dense shielded material behind the Bar.

Key words: ISM: atoms – ISM: molecules – ISM: Orion cloud – ISM: Orion bar – ISM: abundances – radio lines: ISM

1. Introduction

The Orion Nebula, M42, is the closest high mass star formation region. The high ultraviolet flux coming from the hot, young stars in the Trapezium Star cluster, heats and photo-ionises nearby gas, whilst in the core of the cloud, a massive pre-main sequence object, IRc2, drives an energetic highly collimated molecular outflow into the surrounding gas. Several arc minutes south-east of this cloud core, an edge-on ionisation front, the Bright Bar, lies between the expanding rim of the M42 HII region (Martin & Gull 1976; Garay et al. 1987; Yusef-Zadeh 1990) and a dense ridge of molecular gas (Omodaka 1994; Tauber et al. 1994). A narrow ridge detected at infrared wavelengths, traces warm dust along the edge of the Bright Bar facing the Trapezium stars, and shows there is a temperature gradient across this interface (Becklin et al. 1976; Werner 1976; Keene et al. 1982). Observations of the H_2 = 1-0 S(1) line, and the CO, HCO^+ and HCN molecular rotational lines suggest that shocks and uv radiation excite material in the Bar, much of which is relatively warm ($T_{kin} \gtrsim$ 100K - Hayashi et al. 1985; Gatley & Kaifu 1987; Graf et al. 1990; Parmar et al. 1991). This study traces two of the major repositories of carbon inside molecular clouds - CO molecular gas and atomic, CI gas - and compares them to submillimetre continuum emission. The spatial distributions of CO and CI are detectable from ground-based observatories; in this paper observations of the $J = 2 - 1$ CO, ^{13}CO, C^{17}O and C^{18}O, and $J = 4 - 3$ CO molecular rotational transitions are compared with the $^3P_1 - ^3P_0$ atomic fine structure line of CI. Such data can be used to study the relative abundances in the different carbon repositories. The distribution of the gas can also be compared with that of dust; 790 μm continuum observations are reported for the material around IRc2 and the Bright Bar.

2. Observations

The high frequency line observations were taken using the 15m James Clerk Maxwell Telescope (JCMT) during October and December 1993. The 460 - 490 GHz receiver RxC2, used a lead alloy SIS junction that achieved a single-sideband mixer noise temperature of $\sim$ 150K (Ellison 1993) and system temperature T_{sys}, between 930 and 3000K. The CO and isotopomeric $J = 2 - 1$ data were collected with a 205 - 285 GHz SIS receiver, RxA2. All the spectra were calibrated in units of main beam brightness temperature, T_{mb}, correcting for sideband gains, atmospheric attenuation, and the telescope efficiency. The surface accuracy of the JCMT was $\sim$ 30 μm rms, with main beam ef-

Send offprint requests to: Prof. Glenn White

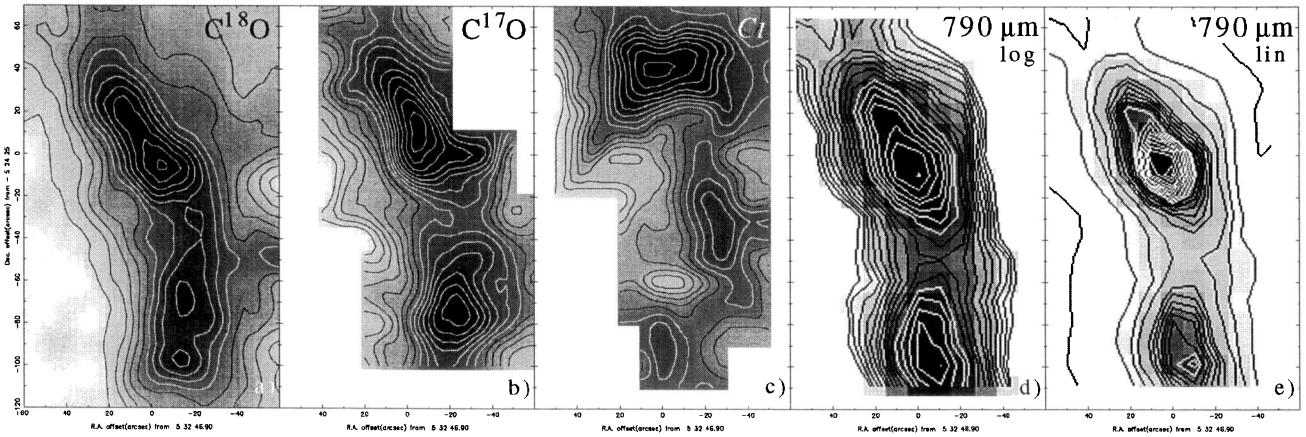

Fig. 1. a Integrated map in the CI line of the OMC1 core. The map contains 153 spectra sampled on a 10 arc second grid, the central (0,0) position being that of IRc2; $\alpha_{1950} = 5^h\ 32^m\ 46.9^s$, δ_{1950} = -05° 24′ 25.7″ , **b** Integrated map in the $J = 2 - 1$ $C^{18}O$ line made from 234 spectra uniformly sampled on a 10 arc second grid, **c** the $C^{17}O$ integrated map made from 132 spectra on a 10 arc second grid, **d** the 790 μm continuum emission with contours plotted on a logarithmic scale, obtained at 2.5 arcsecond spacings, and convolved to a resolution of 10 arc seconds to make the gridding similar to that of the CI data and **e** as for **d** but with contours drawn on a linear scale. For **a–c** the contour interval and first white contours are at (10,70), (5,35) and (1,8) K km s^{-1} respectively, and for the continuum map, where the dynamic range is high, the contours in **d** are logarithmic (in Jy per beam), in units of 0.2, and in **e** linear contours in steps of 2 Jy per beam, with the first white contour at 22 Jy per beam

ficiencies, η_{mb} = 0.72, 0.43 and 0.40 respectively at the CO, ^{13}CO, $C^{17}O$ and $C^{18}O$ $J = 2 - 1$ (230.538, 220.398, 224.714 and 219.560 GHz), CO $J = 4 - 3$ (461.0408 GHz) and CI $^3P_1$ - $^3P_0$ (492.1603 GHz) frequencies. At the highest frequencies, the error beam was ~ 50 arc second radius, with a peak amplitude of 2 % of the diffraction limited beam peak, and contained ~ 40 % of the power. The data were processed with a digital autocorrelation spectrometer, giving spectral resolutions of ~ 0.3 km s^{-1} . The beam sizes at the $J = 2 - 1$ CO, (^{13}CO, $C^{17}O$ and $C^{18}O$ $J = 2 - 1$), $J = 4 - 3$ and CI frequencies were 22, 21.0, 10.5 and 9.8 arc seconds respectively, the pointing was always better than 1 arc second and all observations were made with position switching to a clean off position 2100 arc seconds north of the (0,0) position. Observations of CO and ^{13}CO $J = 2 - 1$ lines made with the same receiver will be presented in more detail in a separate paper by White et al. (1995), however results using the integrated emission and line strengths from these data are used in this paper. Submillimetre continuum observations were made using the UKT14 He^3 bolometric receiver at an effective wavelength of 790 μm . The dual-beam chopped maps, with a beamsize of 13.5 arc seconds, were deconvolved using a maximum entropy analysis technique (Richer 1992). This estimate of the continuum brightness distribution was then re-gridded and convolved with a gaussian restoring beam to accurately match the beam-sizes and sampling of the molecular data - allowing their relative distributions to be compared (the full resolution data will be presented separately (White et al. 1995) - this paper only discusses data smoothed to the resolution of the line data).

3. The data

3.1. CI and $C^{18}O$ $J = 2 - 1$ observations of the IRc2 molecular core region

In Fig. 1 (see the next page) maps of the integrated emission in the CI and the $J = 2 - 1$ $C^{18}O$ lines are shown of the area around IRc2 (this area will be referred to later as the OMC1 core).

The CI emission peaks in two regions lying about 40 arc seconds to the North and South-West of IRc2. These peaks lie at the NE edge of the northern section of the extended ridge (Greaves et al. 1991; White 1992), and are coincident with the southern section of the ridge. The integrated map resembles the distribution first noted in the single velocity map shown by White & Padman (1991), which indicated that CI lay mostly in a shell-like structure around IRc2. Weaker CI emission also peaks at the offset (0, -85) - about 15 arc seconds North of the centre of the southern molecular outflow OMC1-S. CI emission is very weak along the axis of the IRc2 high velocity outflow (running approximately NE-SW through the (0,0) position at $\alpha_{1950} = 5^h\ 32^m\ 46.9^s$, δ_{1950} = -05° 24′ 25.7″).

In this paper, the CI distribution is compared with that of $C^{18}O$, which should be relatively optically thin; this assumption will be justified later. The shape of the $C^{18}O$ map (Fig. 1b) is quite different from that of CI – the only region where both species peak together is close to (-25, -30). The lack of strong correlation between CI and $C^{18}O$ contrasts with the close relationship noted between the two species in M17 (Genzel et al. 1988).

The 790 μm distribution shown in Fig. 1d is more closely correlated with $C^{17}O$ and $C^{18}O$ (Figs. 1c and d). With few exceptions, continuum emission at wavelengths close to 800 μm

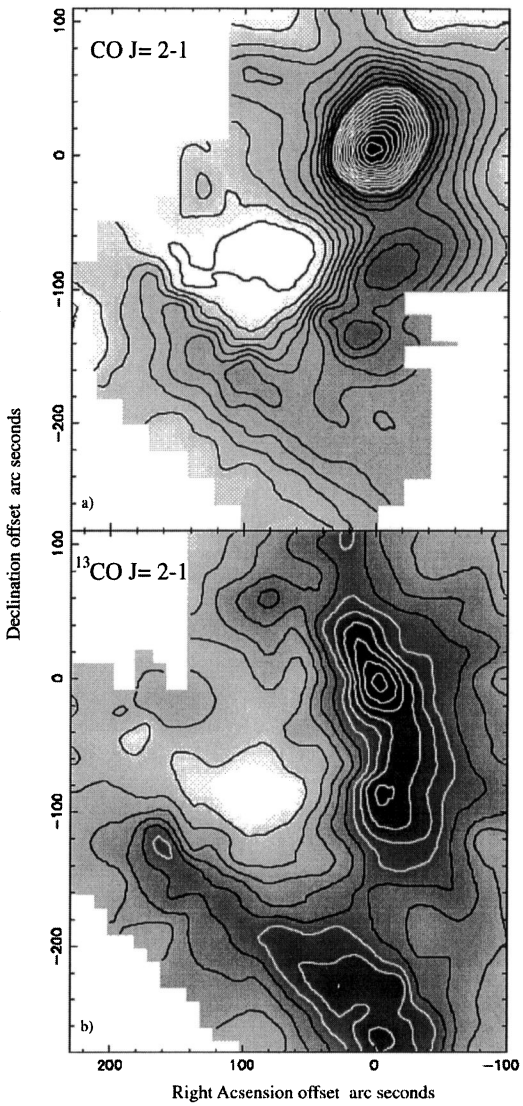

Fig. 2. a Map of the CO $J = 2-1$ line, containing 421 spectra sampled on a 20 arc second grid, **b** map in the ^{13}CO $J = 2-1$ line containing 604 spectra on the similar spacing grid. The contour intervals for the CO and ^{13}CO maps are 40 and 20 K km s^{-1} respectively for the two maps, with the first white contour at 520 and 110 K km s^{-1} respectively. These maps extend beyond the boundaries of the isotopomer maps shown in Fig. 1, and are intended to show the relationship of the Bright Bar to the cloud material associated with IRc2 (which is at the (0,0) position)

from HII region / star-formation complexes is believed to be optically thin (Genzel 1991). It is also likely that C^{18}O and C^{17}O (see Fig. 7) are both optically thin, and can be used to estimate N(CO).

Maps of the molecular distribution in the $J = 2 - 1$ CO and ^{13}CO lines adapted from White et al. (1994) are shown in Fig. 2.

Channel maps of the CI and C^{18}O distributions binned into 1 km s^{-1} intervals, are shown in Fig. 3 (two pages forward) for the region around the OMC1 core.

CI emission in the velocity range between 5 and 6 km s^{-1} is strongest to the South and West of the mapped region. Between 7 and 8 km s^{-1} the emission peaks along a North-South ridge (extending from declination offsets +20 to -70) displaced $\sim$ 20 - 30 arc seconds west of IRc2. This ridge is also prominent in the C^{18}O (Fig. 3b) and ^{13}CO $J = 2 - 1$ lines (Wilson 1986; White et al. 1995 see also Fig. 2 of this paper), and is fragmented into several clumps. Emission immediately to the South of IRc2 is weaker at velocities > 10 km s^{-1}, with a slight enhancement close to offset (20, -50) near the Trapezium cluster. The line intensities are however very weak in this part of the map; firm evidence of any association must await more extensive data.

At ~ 9 km s^{-1}, the velocity of ambient material in the OMC1 core, CI emission does not show a localised peak close to IRc2. At more redshifted velocities ($\gtrsim 10$ km s^{-1}) it peaks towards the northern clump at (+10-20, +50), which is where the highest beam-averaged [CI]/[CO] ratios are seen (see Fig. 10 later). A notable feature of the CI maps is the degree of clumpiness which is present compared to the relative lack of small scale structure in the CO maps.

The C^{18}O maps of the same region (shown in Fig. 3b) appear smoother and less clumpy than those of CI, although the beam width is double that for the CI observations. There are qualitative differences between the maps of the two species at similar velocities: a) CI peaks are often offset from CO cores by 20 - 30 arc seconds, b) relatively strong CI emission is seen from regions where C^{18}O emission is weak, and c) there is little correlation between the peak line temperatures at a given velocity, although the same basic structures are present in both maps.

3.2. *CO $J = 4 - 3$ observations of the IRc2 region*

Figure 4 shows maps of a the peak temperature in a the CO $J = 4 - 3$ line close to IRc2, b the integrated emission, c the red and d blue high velocity wings.

The CO lines around the OMC1 core (Fig. 4a) have main beam brightness temperatures reaching up to $\sim$ 200K, peaking along a narrow ridge centred $\sim$ 10 arc seconds south of IRc2, which extends $\sim$ 40 arc seconds across the map. The CO $J = 7 - 6$ observations of Howe et al. (1993) also show that the peak temperature weakens towards IRc2, however whilst the $J = 7 - 6$ lines are stronger to the North, East and West, the $J = 4 - 3$ lines are more intense in the South. The CO $J = 4 - 3$ lines have a weak absorption feature between 6 and 7 km s^{-1} evident in several of the spectra from the region $\sim$ 10 arc seconds south of IRc2; self-absorption features are not seen elsewhere in the map, nor have they been reported in other single-dish CO observations which were switched far enough away from the source to avoid reference beam contamination.

The gas associated with the IRc2 molecular outflow (Fig. 4c, d) is distributed in two lobes: the blue shifted gas is strongest at the offset position (-6,+6), and the red shifted gas at (+14, -5), with the peaks separated by $\sim$ 25 arc seconds. The blue-shifted lobe is resolved, with a deconvolved diameter of $\sim$ 15 arc seconds; the redshifted peak is more compact, but slightly

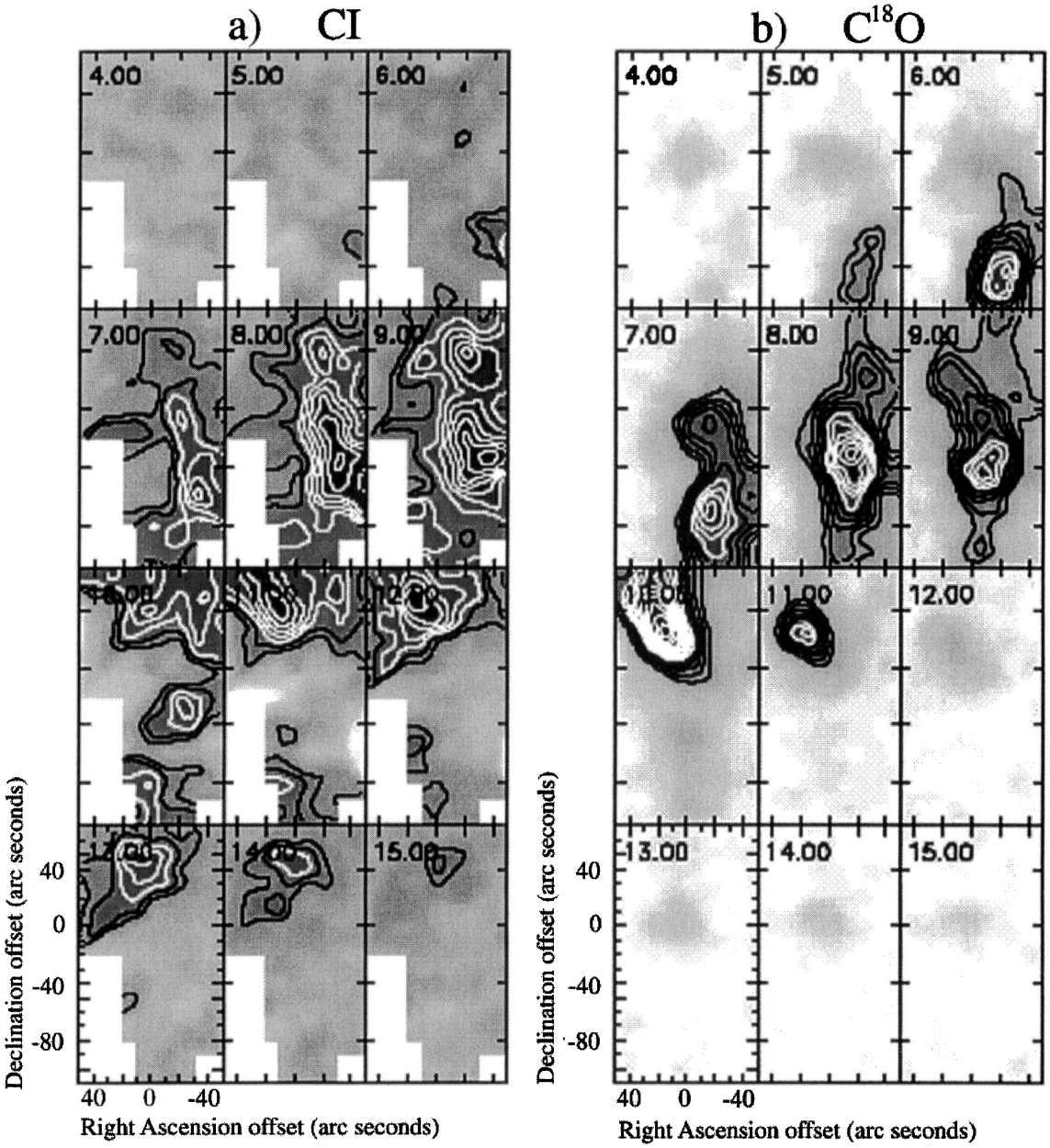

Fig. 3a and b. Channel maps in **a** the CI line, (contour intervals in 2.5 K km s^{-1} steps with the first white contour at 5 K km s^{-1}) and **b** the CO $J = 2 - 1$ C^{18}O lines, with contour steps at 1 K km s^{-1} intervals

elongated along the flow axis. At both peaks low level emission is present from the other velocity range.

The coupling efficiency of the JCMT's main beam at the CO $J = 4 - 3$ line onto a 15 arc second gaussian half-width source, $\eta_c = 0.67$. Correcting the observed spectra to a scale of radiation temperature, T_R, the blue-shifted gas at -10 km s^{-1} has a peak radiation temperature $T_R \sim$ 150K. In the unresolved red-shifted flow, the radiation temperature may be even higher (since η_c will be smaller). These values can be compared with the radiation temperatures estimated from interferometric data for the $J = 1 - 0$ line (Masson et al. 1987) of $\sim$ 60-70K, and in the CO $J = 7 - 6$ (Howe et al. 1993) line of $\geq$ 200K. Since the $J = 1 - 0$ and $J = 4 - 3$ data show the outflow region is actually smaller than was assumed by Howe et al. (they assumed 35 arc seconds), their estimated temperatures may need to be increased by an further factor of 2 - 3. Qualitatively the CO line temperatures increase with rotational transition, but the uncertainties in the various coupling corrections are relatively large. The data confirm the presence of substantial amounts of hot ($T_{ex} \gtrsim$ 150 - 200 K) CO in the outflowing gas, supporting the upper bound of the estimate of Graf et al. (1990) of 80 - 250K. In the $J = 2 - 1$ transition, emission from the CO line wings is almost certainly optically thick (since theC^{18}O lines

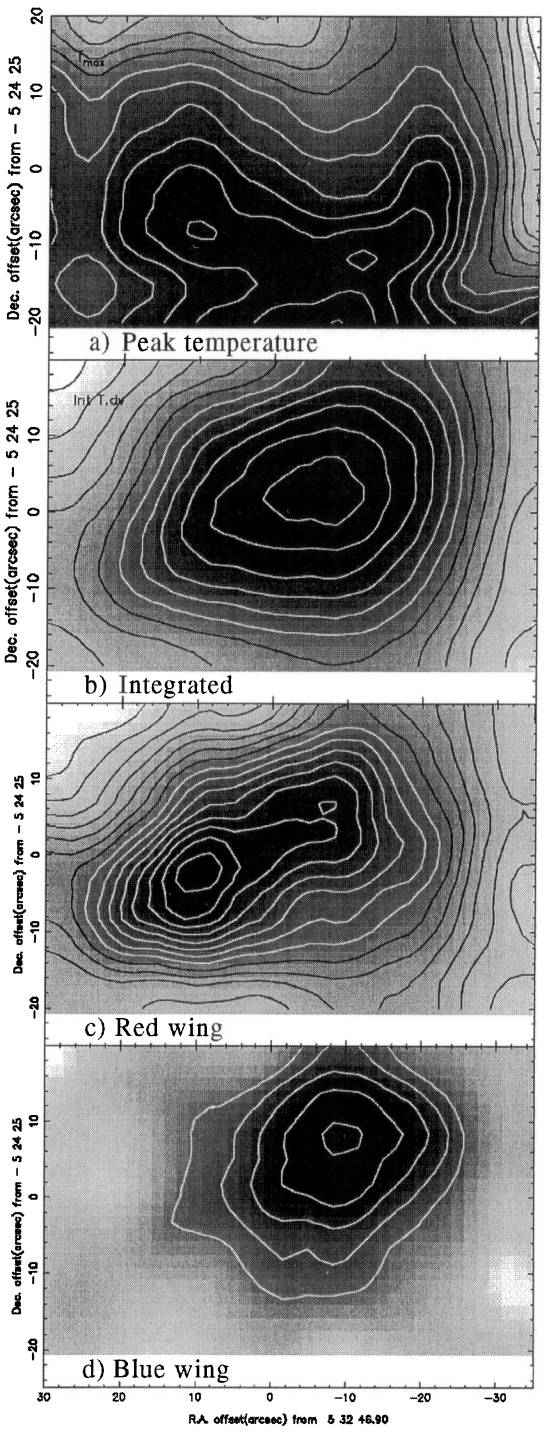

Fig. 4a–d. Maps of **a** the peak CO $J = 4 - 3$ emission (-75 to +85 km s^{-1}), with contours of main beam brightness temperature every 5 K, and the first white contour at 120 K **b** the integrated emission with contour intervals of 500 K km s^{-1} and the first white contour at 4000 K km s^{-1}, **c** in the red (25 to 75 km s^{-1}) and **d** blue (-25 to -75 km s^{-1}) line wings, with contours every 50 K km s^{-1} and the first white contours at 500 K km s^{-1} intervals

extend to at least $\pm$ 20 km s^{-1} from the ambient velocity of the cloud - suggesting high optical depths in the CO lines).

3.3. CI and CO observations of the Bright Bar ionisation front

Maps of integrated emission towards the Bright Bar in the CO $J = 4 - 3$ and C I lines are shown in Figs. 5 a and b, in c the C I is overlaid onto the CO map, and then compared with the 10 μm , H_2 and 3.3 μm (which is believed to trace PAH molecules) distributions in Fig. 5 d and e.

The CO $J = 4 - 3$ emission extends over the velocity range $\sim$ 6 to 14 km s^{-1} ; the lines are single peaked, with half-widths $\sim$ 4 - 6 km s^{-1}, peaking between lsr velocities of 10 and 11 km s^{-1}. A small red shift ($\sim$ 2 km s^{-1}) of the gas in the Bar (relative to nearby molecular material) has been suggested as evidence for expansion of the HII region around the Trapezium cluster, which then drives a shock into the bar - forming a narrow ridge of heated and compressed material (Omodaka et al. 1994). Spectra taken along their strip confirms the velocity shift (see their Fig. 2), but the present data do not show evidence for a systematic shift along the whole extent of the Bar; instead the Bar is highly clumped, and the velocity 'shifts' are probably associated with this inhomogeneous structure. The CO $J = 4-3$ main beam brightness temperatures are $\geq$ 175 K in places, again showing there is a substantial amount of warm gas present (cf. $\sim$ 30 % of the total gas mass - Graf et al. 1990).

The CO $J = 4 - 3$ map (Fig. 5a) appears to be more clumpy than the high resolution CO $J = 1 - 0$ map obtained using the BIMA interferometer (Tauber et al. 1994). Four hot-spots can be seen at offsets (-15, -15), (-36, -32), (-46, -43) and $\sim$ (-80, -60), lying along a narrow bar at the edge of the ionisation front. The CO line intensity drops off sharply to the NW, in the direction toward the illuminating stars in the Trapezium cluster. The 10 μm bar (Becklin et al. 1976), which traces heated dust grains, lies offset from the CO and C I ridges (Fig. 5d) by $\sim$ 15 arc seconds (see Fig. 5e) towards the Trapezium cluster. This IR bar approximately coincides with the 3.3 μm ridge that is believed to trace the distribution of PAH molecules (Burton et al. 1991). It is noticeable (see later) that the 790 μm emission from this region is also clumpy (Fig. 12b). The BIMA CO $J = 1 - 0$ peak intensity is $\sim$ 95 K; similar to T_{mb} values obtained with the Nobeyama 45m telescope (beamsize 15 arc seconds) of $\sim$ 90 K (unpublished data). The CO $J = 4 - 3$ lines are brighter than either of the $J = 1 - 0$ lines by a factor of $\sim$ 2, showing the same trend as seen in the IRc2 region.

In Fig. 5b, the C I ridge stands out clearly above the surrounding gas, although some of the peaks appear to be offset from the $J = 1 - 0$ ^{13}CO hot-spots by $\sim$ 5 - 10 arc seconds (this needs to be confirmed with better sampled data). Some C I emission is also coincident with the compact HCO^+ peak (at offset (-71, -50)) measured by Tauber et al. (1994). It therefore appears, on morphological grounds, that although some of the C I is well mixed with other material in the Bar, a significant fraction of it may come from material close to the surface layers of clumps which are illuminated by the uv flux coming from the Trapezium stars. Similar conclusions have been reached for

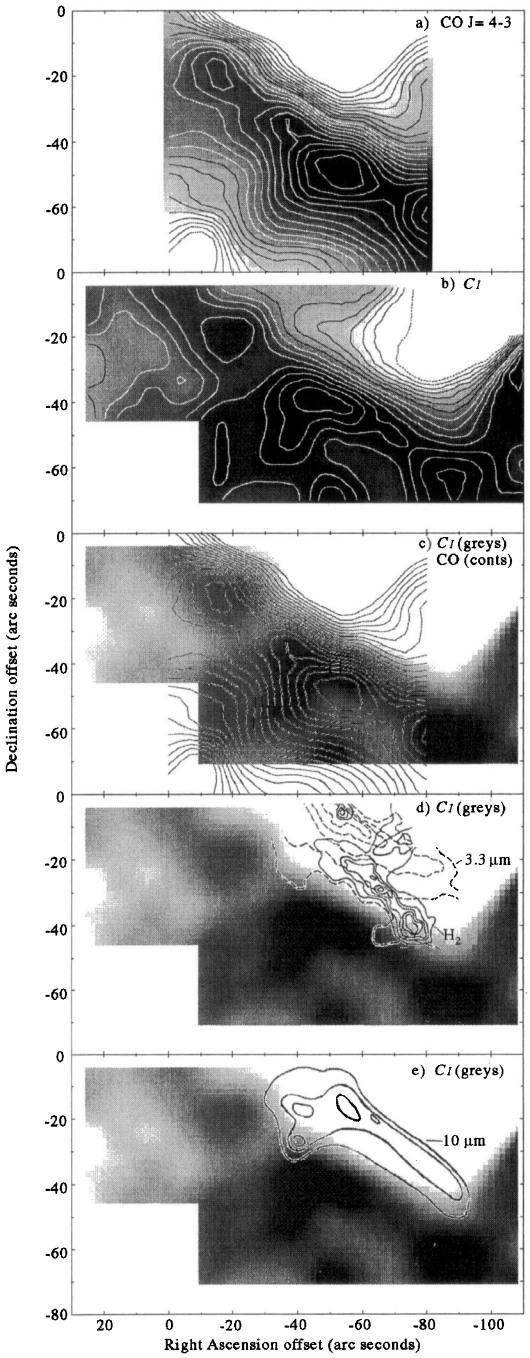

Fig. 5a–e. Maps of the Bright Bar **a** the integrated CO main beam brightness temperature, with the first white contour at 530 K km s^{-1} and steps of 33 K km s^{-1}, **b** the integrated $^3P_1 - {}^3P_0$ CI emission over the velocity range 4 to 14 km s^{-1} with the first white contour at 30 K km s^{-1} with steps of 5 K km s^{-1}, **c** the CO $J = 4-3$ contours overlaid on the CI greyscale image, **d** the CI (greyscale) overlaid with the H_2 and 3.3 μm distributions of Burton et al. (1990) and **e** the 10 μm bar of Becklin et al. (1976) overlaid on the CI greyscale image. The centre position of the maps is at $\alpha_{1950} = 5^h\ 32^m\ 57.8^s$, $\delta_{1950} = -05^o\ 26'\ 26''$

the M17SW ridge, which is also externally illuminated by an OB star cluster (Hobson et al. 1994).

4. Discussion

The data collected in this study can be used to examine the relative abundance variations of CO and CI. The CO isotopomeric column densities (in units of cm^{-2}) may be estimated using the emission from a line (such as the $(J + 1)$ to J transition of an optically thin(ner, than CO) isotopomer), with the relationship which has been commonly used, in various forms, by many workers in the past;

$$N_{col} = \frac{3.3410^{14} \int T_{mb} dV}{\nu\mu^2 \left(1-e^{-\frac{h\nu}{kT_{ex}}}\right)\left(e^{-\frac{Jh\nu}{2kT_{ex}}}\right)} \frac{\tau}{1-e^{-\tau}} \quad (1)$$

where T_{ex} is estimated from the peak CO $J = 2 - 1$ main beam brightness temperature, $\int T_{mb}$ dV is the isotopomer's main beam brightness temperature integrated over the line width in K km s^{-1}, J is the lower rotational quantum number (1 for the CO $J = 2 - 1$ transition), ν is the line frequency (in GHz) and μ is the dipole moment (in Debye's). The opacity, τ, is estimated using the peak intensity of the line T_{peak} and the CO peak temperature T_{kin}, from the relationship;

$$T_{peak} \cong \frac{h\nu}{k} \frac{(1-\exp(-\tau))}{\left(\exp\left(\frac{h\nu}{kT_{kin}}\right)-1\right)} \quad (2)$$

Equation 1 assumes that the Planck corrected CO peak temperature is the same as the kinetic temperature (which is then assumed to be equal to the excitation temperature, and constant for all the CO rotational levels), that the isotopomer is in LTE, and that the escape probability $\beta = \tau / (1\text{-}e^{-\tau})$ can accurately account for optical depth effects.

It is questionable whether a single value of excitation temperature is applicable to CO and its isotopomers, although this assumption, or some arbitrary choice, has been used in the past to estimate the abundance ratios of [CI]/[CO], averaged over the particular telescope beam. Multi-line CO observations with large beams (in the range 100 - 140 arc seconds) have been successfully explained in the framework of uv-penetrated clumpy clouds, with clump densities up to $N(H_2) \sim 10^5$ cm^{-3}, and strong temperature gradients which affects the relative excitation temperatures of different isotopomers (Castets et al. 1990). Recent theoretical work (Köster et al. 1994) modelling the emission of a cloud containing several clumpy photon dominated regions (PDR's), has confirmed that a wide range of excitation temperatures co-exist throughout the emitting regions; making any simple interpretation with a single excitation temperature T_{ex} unrealistic. This treatment also showed that isotopic fractionation of ^{13}CO should occur in these regions. For further discussion of choosing T_{ex}, and the errors and difficulties involved, the reader is referred to Dickman (1978), Tauber et al. (1994) and Köster et al. (1994).

The situation with choosing T_{ex} (CI) is also unclear. In the two cases where both the $^3P_2 - {}^3P_1$ and $^3P_1 - {}^3P_0$ lines of CI have been observed (Orion and M17 - Jaffe et al. 1985; Zmuidzinas

et al. 1988; Hobson et al. 1994) the line ratios point towards high values for T_{ex} . This can be understood if the CI emission comes from hot gas in an interclump region, or from the photo-dissociated edges of cooler clumps (see also Meixner & Tielens 1993). If this is the case, then the CI lines may appear optically thin, and N(CI) will only be a weak function of temperature - the inferred column densities changing by $\lesssim 10$ % over a wide range of temperatures (assuming $T_{kin} \gtrsim 30$K). There would however be interpretational problems if the CO isotopomers and CI come from physically distinct gas masses - it is not immediately obvious how this can be resolved from the present data - an improved understanding of this omni-present problem of many molecular line studies awaits direction from improved modelling techniques.

To establish whether the column densities inferred from individual CO isotopomeric data are reliable indicators of N(CO), estimates were made using the $J = 2 - 1$ $C^{18}O$ and $C^{17}O$ (this paper) and the CO and ^{13}CO lines (White et al. 1995) at each point in the maps. Assuming that the isotopomers have the same excitation temperature as CO (see discussion earlier), then with first order corrections for opacity the data should yield similar CO column densities when multiplied by the relative isotopomeric conversion factors (see caption of Fig. 6). To illustrate this, results are shown in Fig. 6 for N(CO) derived from the present ^{13}CO and $C^{18}O$ data.

The CO column densities inferred using ^{13}CO and $C^{18}O$ data differ by factors of ~ 2 or more in the region around IRc2 over the range 10^{18} - 3 10^{19} cm^{-2} - in the sense that $C^{18}O$ is *underabundant*, or that ^{13}CO is *overabundant*. These column densities correspond to visual extinction, A_v values of $\sim$ 15 - 160 magnitudes using the standard relationship $N(H+2H_2)/A_v \approx 1.9\ 10^{21}$ atoms cm^{-2} , and X(CO) = 10^{-4}(Bachiller & Cernicharo 1986; Keene 1987). However, for the Bright Bar data, ^{13}CO appears *underabundant* relative to $C^{18}O$ at the higher column densities, and *overabundant* at lower column densities. This lack of agreement between the column densities inferred from the two isotopomers could be due to one or more of several factors; a) $C^{18}O$ may sample material deeper into the cores of clumps than do the ^{13}CO lines, b) CO and isotopic abundance ratios may be influenced by photoionisation (see discussions by Dutrey et al. 1993; Köster et al. 1994), c) fractionation of one isotopomer is more dominant than for others, d) assumptions of a similar T_{ex} for all isotopomers are inappropriate, or e) that radiative trapping has not been correctly accounted for. By contrast, the N(CO) values towards the Bright Bar region show better agreement than the data towards the IRc2 cloud. The importance of ^{13}CO fractionation is discussed in the next section.

In a similar study of CO isotopes to the present one, White et al. (1995) analysed a similar multi-transition data set for the cooler dark cloud associated with the Serpens star cluster. Based on comparative modelling of $C^{18}O$ data using LVG and LTE analyses, the deduced column densities for warm material such as that likely to be present in the OMC1 cloud and Bright Bar ($T_{kin} > 20$ K and densities $> 10^3$ cm^{-3}) are in approximate (factors of two or three) agreement. However, at lower temperatures and low densities, the deduced column densities disagree by up to one order of magnitude - even a rare isotopomer such as the $J = 2 - 1$ $C^{18}O$ line does not in fact accurately trace column density in cool dark clouds. A fuller discussion of this problem is beyond the scope of the present paper, and will be given by White et al. (1995), but on the basis of this modelling it does not appear unreasonable to use an LTE approach for the OMC1 cloud and Bright Bar, as we have done here.

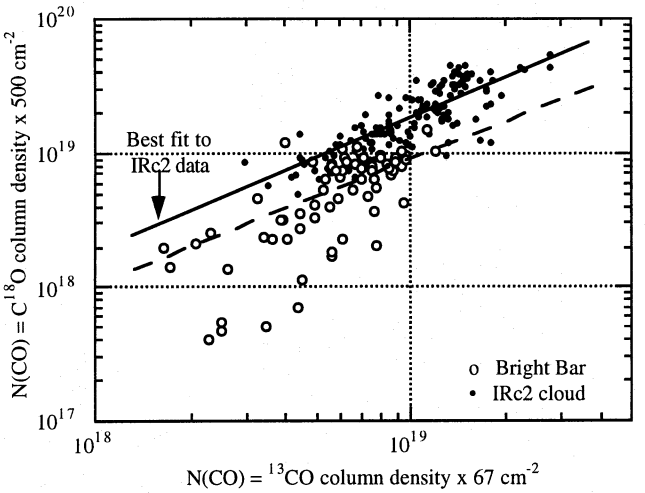

Fig. 6. Comparison of N(CO) derived from the ^{13}CO and $C^{18}O$ column densities multiplied by the canonical abundances relative to CO of 67 and 500 respectively (Gierens et al. 1992). The top model fit line is a least square fit (extrapolated) to the IRc2 cloud data (only) (i.e. with a terrestrial isotope ratio [CO/[$C^{18}O$] = 500), and the lower model line (dashed) shows the expected fit if both isotopomers traced the same value of N(CO)

Several studies have suggested that the ratio of ^{13}CO to $C^{18}O$ can exceed the terrestrial ratio (5.5) because of $C^{18}O$ photodissociation, and chemical fractionation of ^{13}CO (van Dishoeck & Black 1988; Turner et al. 1992; Turner 1993; Fuente et al. 1993; Köster et al. 1994). The ratio N(^{13}CO)/N($C^{18}O$) has been shown to exceed the terrestrial value close to the surfaces of several dark clouds (Frerking et al. 1982; Bachiller & Cernicharo 1986 and Lada et al. 1994). Taking the relationship between N($C^{18}O$) and A_v from Lada et al. (1994), which have been determined for A_v up to 15 magnitudes, the ratio N(^{13}CO) / N($C^{18}O$) against extinction in the Orion region is shown in Fig. 7 (note: in the present paper the values of A_v have been extrapolated to higher values than Lada et al. 's relationship has been measured over, the validity of this is examined later).

In Figs. 7b and c the data for the OMC1 clouds and the Bright Bar are shown separately. For Fig. 7b the relationship N(^{13}CO) / N($C^{18}O$) = 26 $A_v^{-0.37}$ with a correlation coefficient of 0.58, and for 7 c), the relationship N(^{13}CO) / N($C^{18}O$) = 90 $A_v^{-0.62}$ with a correlation coefficient of 0.91. The merged data shown in 7 a) are dominated by the Bright Bar data, which provide strong evidence for ^{13}CO fractionation. The case for a ^{13}CO overabundance in the OMC1 core is less convincing, the

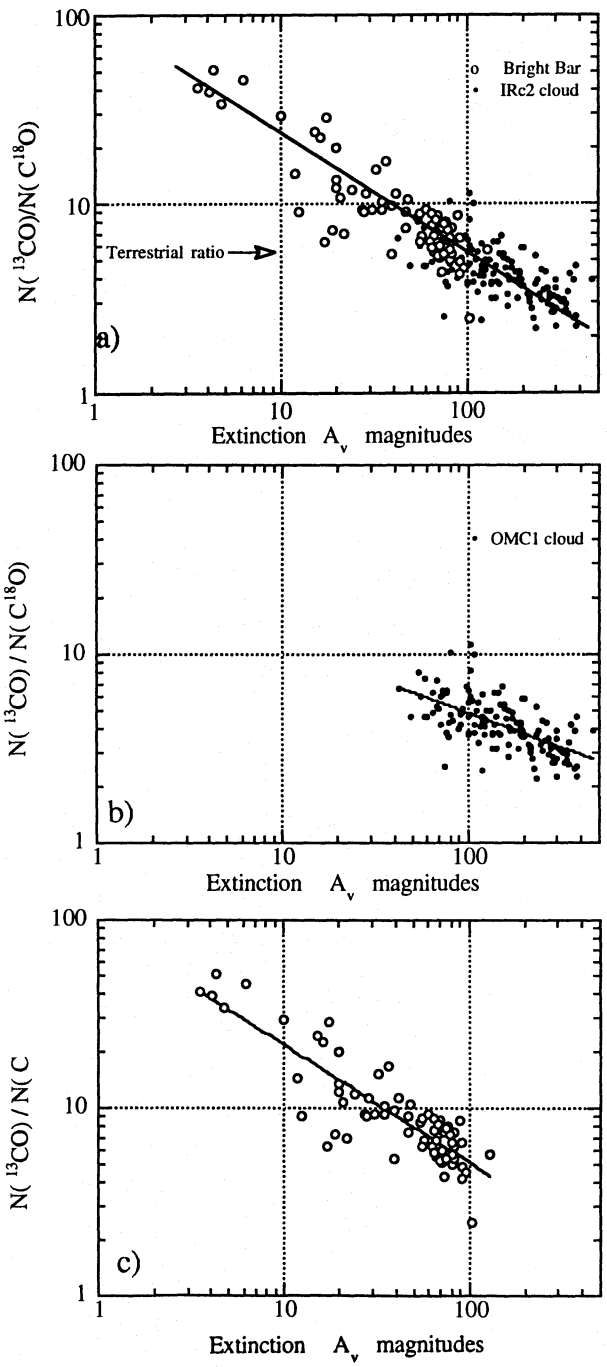

Fig. 7a–c. Graphs of $N(^{13}CO)/N(C^{18}O)$ against extinction as estimated from the $C^{18}O$ data. In **a** the merged data from the OMC1 cloud and the Bright Bar are shown together. The best fit power law shown is for the relationship $N(^{13}CO)/N(C^{18}O) = 80\ A_v^{-0.6}$ with a correlation coefficient of 0.91

observed characteristics may instead be a consequence of high ^{13}CO opacity.

These data show that $N(^{13}CO)/N(C^{18}O)$ exceeds the terrestrial ratio for $A_v \lesssim 40$ magnitudes, with the highest values occurring towards positions in the Bright Bar (where the photoionisation levels are high and A_v is lower). Fractionation is expected to occur mostly in the first few A_v of a cloud's surface (van Dishoeck & Black 1988). That it seems to extend far more deeply into the cloud can be best understood within the framework of a clumpy cloud model - fractionation occurring on the surfaces of more deeply embedded clumps. At the higher extinction values, the column density ratio is about half of the terrestrial ratio - possibly a consequence of saturation of the ^{13}CO, which may not have been completely corrected for by the $\tau/(1\text{-}e^{-\tau})$ correction factor in Eq. 1. If T_{ex} (^{13}CO) has in fact been overestimated, τ (^{13}CO) will increase, and $N(^{13}CO)$ will be a strict lower limit. Detailed modelling beyond the scope of this work would be required to comment further on how this would modify Figs. 6 and 7.

Dutrey et al. (1993) have also noted for Orion that ^{13}CO data may lead to under-estimates of CO column densities compared to those inferred from $C^{18}O$ data, by factors of up to 5 - 10 (although they do not discuss its dependence on extinction). The present data provide substantial support for ^{13}CO fractionation; a trend convincingly observed in the dark cloud B5 (Young et al. 1982). Specifically the ^{13}CO becomes saturated on the outer surface layers of clumps, whilst $C^{18}O$ molecules require a larger H_2 column density in front of them before a substantial number can survive against photodissociation. Thus the $C^{18}O$ data sample material at a greater depth (than ^{13}CO), and hence may measure a different column density to that estimated from ^{13}CO data. In a simplistic model, the CO data trace the low density halo or external envelope of the cloud, the ^{13}CO data trace the cloud to intermediate depths, and the $C^{18}O$ originates from throughout the cloud. The $C^{18}O$ data is almost certainly a better tracer of the column density throughout most of the cloud, consequently in this paper estimates of [CI]/[CO] will be based on the use of $C^{18}O$ data to infer N(CO). As further support for this assertion, we will show later that there is also a correlation between $N(C^{18}O)$ and the 790 μm continuum emission, which is believed to be completely optically thin.

It is important to determine whether fractionation only affects the ^{13}CO abundances, or also affects other CO isotopomers. To test this, a similar analysis was applied to the rarer $C^{18}O$ and $C^{17}O$ lines. In Fig. 8, the ratio $N(C^{18}O)/N(C^{17}O)$ versus A_v shows a relatively constant ratio of 3 - 5 (compared with the terrestrial $[^{18}O]/[^{17}O]$ ratio of 5 - Anders & Grevesse 1989, and the interstellar value ~ 3.7 - Penzias 1981). There is a weak trend for this ratio to decrease at lower A_v values. This result shows that the effect seen in Fig. 7 is almost entirely due to ^{13}CO fractionation, rather than being a consequence of $C^{18}O$ depletion or fractionation. This has important implications for cloud mass estimates. It has been common practice for CO column densities to be estimated using CO and ^{13}CO data alone - then by assuming a constant $X(^{13}CO)$ to infer n_{H2}. The present data show that fractionation does lead to a substantial increase in

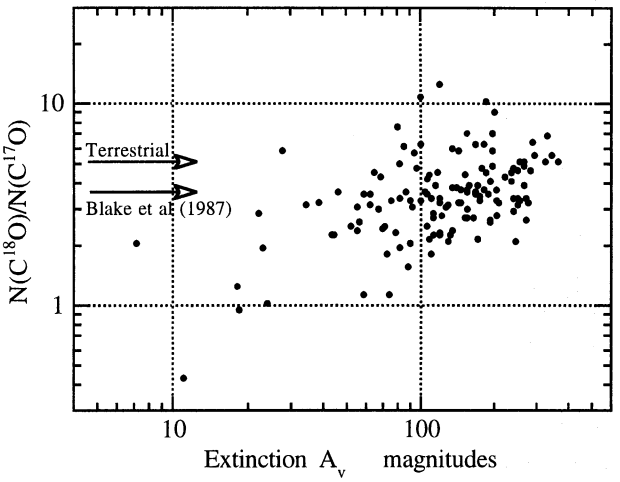

Fig. 8. Graph of $N(C^{18}O)/N(C^{17}O)$ against extinction. This graph only contains points for the IRc2 cloud - no $C^{17}O$ data are available for the Bright Bar region. The detections of the weak $C^{17}O$ lines all have reasonable signal to noise ratios - it is unlikely that the trend above is due to low s/n values for the smaller A_v points

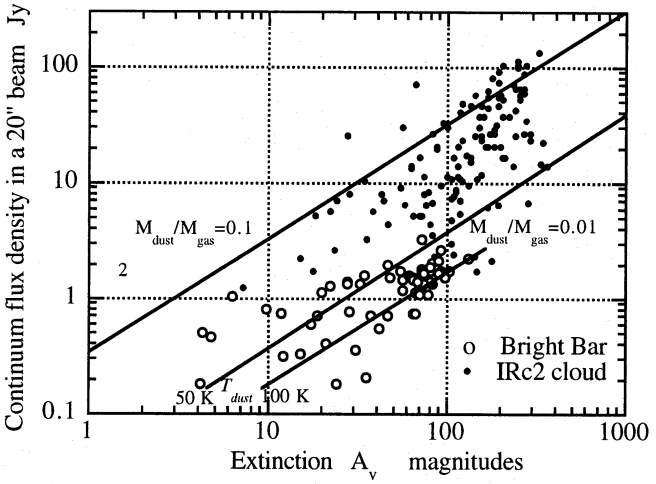

Fig. 9. Graph of the 790 μm flux density convolved to a 20 arc second beam, against $A_v$determined from the $C^{18}O$ data, assuming the Lada et al. (1994) relationship. The model fits show lines of constant M_{dust}/M_{gas} for an assumed dust temperature = 50K, and grain emissivity, β =1.5 (following Wright et al. 1992). The M_{dust}/M_{gas} line is further subdivided for values of T_{dust} = 50 K and 100 K. The present data do not modify the results of Wright et al. (1992), however it is likely that a choice of β = 2 may be more appropriate for the Bright Bar, where it is expected that the grains may not be so covered as those in the OMC1 cloud. Further observational data are however needed to resolve this issue

X(^{13}CO), with the consequence that many cloud mass estimates may need to be revised downward to allow for it.

Figure 8 shows that for most points, the observed isotopic ratio is lower than the terrestrial ratio, as was also reported by Blake et al. (1987) towards the OMC1 core. There is a weak trend for the $N(C^{18}O)$ / $N(C^{17}O)$ ratio to decrease towards lower A_v, although further data at lower A_v values is needed to assess the significance of this. It is however clear that the enhancement seen in the ^{13}CO abundances at lower A_v values, is not seen in the $C^{17}O/C^{18}O$ data when analysed in a similar way.

Submillimetre continuum data at 790 μm were convolved to the same beamsize and gridding as the molecular data, and compared with the isotopomeric column densities. In Fig. 9, a graph is shown of the submillimetre continuum flux density plotted against A_v (which is proportional to the $C^{18}O$ column density). The result for $C^{17}O$ shows a similar trend.

There is a weak correlation between the 790 μm continuum flux and $N(C^{18}O)$ extending over $\sim$ 2 orders of magnitude in A_v and almost 3 orders of magnitude in 790 μm flux density. However, the spread of values is quite large, and the Orion Bright Bar data lie systematically lower than the data points seen in the OMC1 cloud. These data do however give some support to the assumptions made in this paper that Lada et al. 's (1994) relationship can be extrapolated to higher A_v's than their study traced. However, similar studies to this will need to be made towards other regions to give substance to such an extrapolation.

The dust/gas mass ratio can be examined with these data - an important feature of which is that they are probably both relatively optically thin. The dust mass, M_{dust} (in $M_\odot$ units) for a source at a distance D parsecs and flux density S_ν (in Janskys) can then be estimated using the relationship;

$$M_{dust} = 1.8810^{-10} \left(\frac{S_\nu}{Jy}\right) \left(\frac{1200}{\nu}\right)^{3+\beta} \left(e^{\left(\frac{0.048\nu}{T_{dust}}\right)} - 1\right) D^2 \quad (3)$$

Lines showing constant gas/dust mass ratios are indicated on Fig. 9, for an assumed dust temperature T_{dust} = 50 K and a grain emissivity β = 1.5 (values representative of the material in the OMC1 cloud - Wright et al. 1992). For other nearby choices of dust parameters, the flux density scales $\propto 1/T_{dust}$ and $\propto \beta$. No corrections were made for any molecular line emission contained in the continuum pass band; this may contribute as much as 25 - 40 % of the total broad-band flux at the position of IRc2 - but is probably negligible in other parts of the cloud (Sutton et al. 1985; Greaves & White 1991). Most of the data from the OMC1 cloud shows a dust/gas mass ratio averaging $\sim$ 2 - 4 %. This is somewhat higher than the canonical ratio of $\sim$ 1 % - which has been determined mainly at the centres of dense cores in molecular clouds - the present result is more representative of the widespread cloud material. We stress that a major source of uncertainty which remains is a lack of knowledge of the dust temperature and of β. The Bright Bar data seem to form a different population from the OMC1 cloud data. Their position in Fig. 8 is consistent with them being hotter, and having a higher β value, which would indicate grain material that was not yet covered with an organic mantle. Such a scenario may be appropriate for the dust in the Bright Bar, which is experiencing strong shocks and uv irradiation, however we again caution that these tentative conclusions rely heavily of guesses at the dust temperature and of β.

The excitation temperature in the C I line remains uncertain. A lower limit can be set by comparing the intensities at the peaks of the $^3P_1 - {}^3P_0$ and $^3P_2 - {}^3P_1$ lines - as was attempted by Zmuidzinas et al. (1988). Their best estimate for T_{ex} (C I) = 77 K

was derived by comparing the spectra for the two lines obtained with 150 and 80 arc second beams respectively, and making assumptions as to how to correct their data for reference beam emission. Using the present CI data, it is possible to make a more accurate estimate of the excitation temperature using matched beams. The JCMT CI data were convolved to a resolution of 80 arc seconds, to match the beamsize of Zmuidzinas et al. 's CI data - removing the need to correct for different beam sizes. The peak line intensities of the $^3P_1 - {}^3P_0$ and $^3P_2 - {}^3P_1$ spectra, $T_{mb} = 12.5$ and 9.7 K respectively. Correcting Zmuidzinas et al. 's spectrum for reference beam emission (as described in their paper), T_{ex} (CI) can be solved numerically from the relationship;

$$1.28e^{-\frac{23.6}{T_{ex}}}\frac{1-e^{-\frac{38.8}{T_{ex}}}}{1-e^{-\frac{23.6}{T_{ex}}}} = \frac{\ln\left\{1-\frac{T_{mb2}\left(e^{\frac{38.8}{T_{ex}}}-1\right)}{38.8}\right\}}{\ln\left\{1-\frac{T_{mb1}\left(e^{\frac{23.6}{T_{ex}}}-1\right)}{23.6}\right\}} \quad (4)$$

This assumes that the excitation temperature is the same for both lines, and that $T_{mb\,1}$ and $T_{mb\,2}$ are the peak main beam brightness temperatures of the lower and upper transitions. Solving this equation, the best fit value of T_{ex} for CI is found to be $\gtrsim 90$ K. Varying the intensity of either of the spectra by 10 % leads to a 10 - 20 % change in T_{ex}. The optical depths of the lower and upper lines are $\tau = 0.27$ and 0.39 respectively. To test the assumption of equal excitation temperatures for both lines, an LVG model was run using the data to examine this in more detail. The ratio of the excitation temperatures of the two transitions is relatively insensitive to the gas density, and varies by less than $\pm$ 20 % over a range of $\sim$ 1 order of magnitude in density, for conditions appropriate to the Orion molecular cloud.

The CO $J = 2 - 1$ data were convolved to the same 80 arc second resolution as Zmuidzinas et al. 's CI $^3P_2 - {}^3P_1$ spectrum; the value of T_{mb} (CO) = 108 K, which for optically thick emission, suggests that the beam-averaged $T_{kin} \sim 110$ K. Therefore, to first order, for the purpose of inter-comparison of the beam-averaged large scale distribution of CI and the CO isotopomers, it appears reasonable to set T_{ex} (CI) $\sim T_{kin}$ (CO) - although it is not certain that this approximation is appropriate to make when modelling small scale structure within a cloud. This agrees with the framework of the model of Meixner & Tielens (1993), in which the low J CO lines and the CI lines come from similar interclump regions. Henceforth in this paper, it will be assumed that T_{ex} (CI) is equal to T_{ex} (CO).

The beam-averaged CI column density, N(CI) can then be calculated using the relationship given by Keene et al. (1986);

$$N(CI) = 1.9\,10^{15}\left\{e^{\frac{23.6}{T_{ex}}}+3+5e^{-\frac{38.0}{T_{ex}}}\right\}\frac{\tau}{(1-e^{-\tau})}\int T_{mb}dv \quad (5)$$

For typical values found for the CI data, setting T_{ex} (CI) = 0.5 T_{ex} (CO) or up to 5 times T_{ex} (CO), results in changes to N(CI) of $\lesssim 10\%$ - therefore the CI column density estimates are not very sensitive on T_{ex}, except where it is needed to calculate

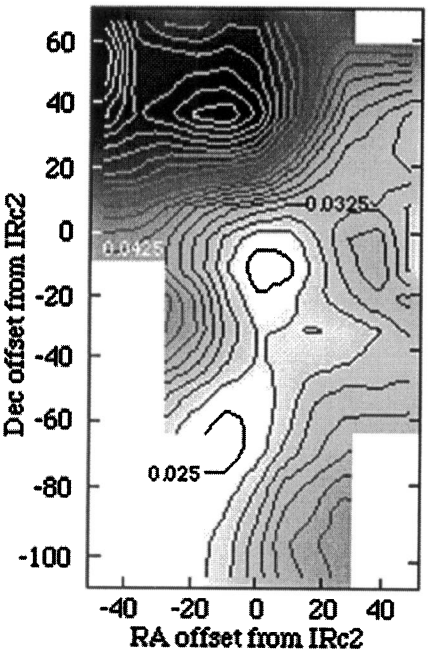

Fig. 10. Map of the beam-averaged abundance ratio [CI]/[CO] around the position of IRc2. The contour intervals are in units of 0.005 (in [CI]/[CO]) superimposed on a greyscale image with the darker portions representing higher values, where the ratio reaches up to 0.12

the opacity (the CI opacity is assumed to be ≤ 1 in this paper as seems to be the case towards other high-mass star-formation regions). The N(CI) estimates at each point in the map can then be used with N(CO) to examine the beam-averaged abundance ratio [CI]/[CO]. A map of this ratio is shown in Fig. 10.

The minimum value of this ratio occurs $\sim$ 10 arc seconds south of IRc2, close to the position of the 'hot core', where the densities and temperatures are believed to be very high. The south western CI peak seen in the integrated intensity map (Fig. 1a) does not show an enhanced [CI]/[CO] ratio, the highest values in fact come from the north eastern peak. This lies on the northern section of the extended ridge, at the edge of several small clumps seen in the CS $J = 2 - 1$ lines by Murata (1992).

A map of the ratio [CI]/[CO] towards the Bright Bar ionisation front is shown in Fig. 11 (see over the page).

The present data set can be used to examine the variation of [CI]/[CO] with the CO peak line temperature, and with A_v. In Fig. 12, the abundance ratio [CI]/[CO] is plotted against the CO excitation temperature T_{mb} (CO).

The values of [CI]/[CO] show a weak trend to decrease towards the higher CO peak temperatures with a power law relationship where [CI]/[CO] $\propto T_{ex}$ (CO)$^{-2.8}$; the higher ratios occurring in cooler gas, and close to the Bright Bar. The abundance ratio [CI]/[CO] is plotted against CO column density in Fig. 13.

This shows a good fit to a power law, with a slope similar to that seen in the data of Frerking et al. (1989) obtained towards ρ Oph. Extrapolating the fit to the data in Fig. 13 to lower column densities, the extrapolated curve matches closely with values

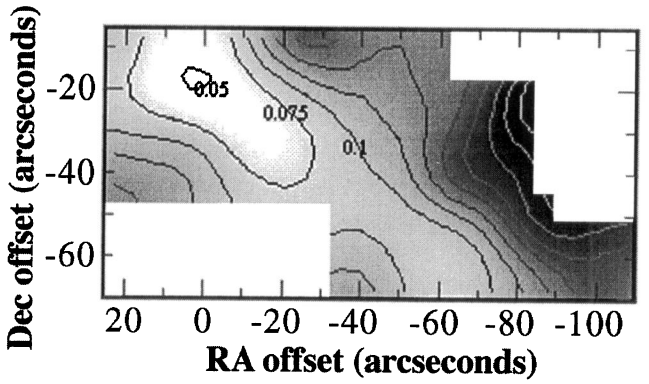

Fig. 11. Map of the variation of [CI]/[CO] with N(CO) estimated from the $C^{18}O$ data. The contours are in steps of 0.05. The darker grey scales indicate a higher ratio of [CI]/[CO]. Thus the Bright Bar is seen as a *minimum* in the ratio of [CI]/[CO]. Although there is a clear minimum towards the NE part of the Bar, the ratios still remain high over most of the region. This map can be compared with the larger scale structure of the Bar which is shown later in Fig. 14. The (0,0) position for this map and that of Fig. 14 is $\alpha_{1950} = 5^h\ 32^m\ 57.78^s$, $\delta_{1950} = -05^o\ 26'\ 20.0''$

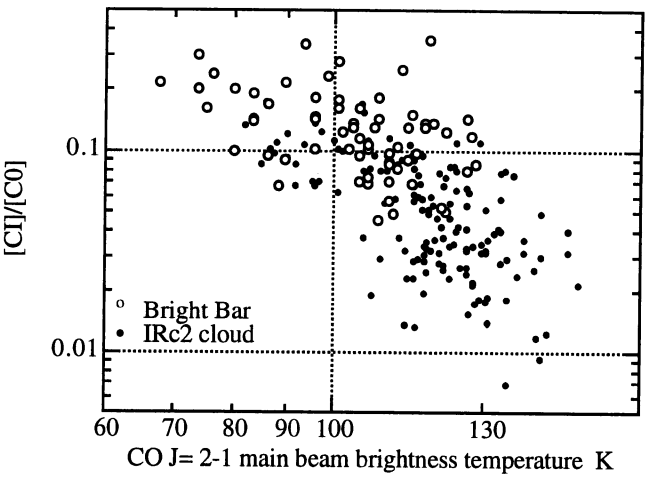

Fig. 12. Plot of the beam averaged abundance ratio [CI]/[CO] and the CO $J = 2 - 1$ peak temperature for the cloud around IRc2, and the Bright Bar ionisation front. The best fit power law gives a relationship $[CI]/[CO] = 3.7\ 10^4\ T_{mb}\ (CO)^{-2.8}$, with a correlation coefficient of 0.62

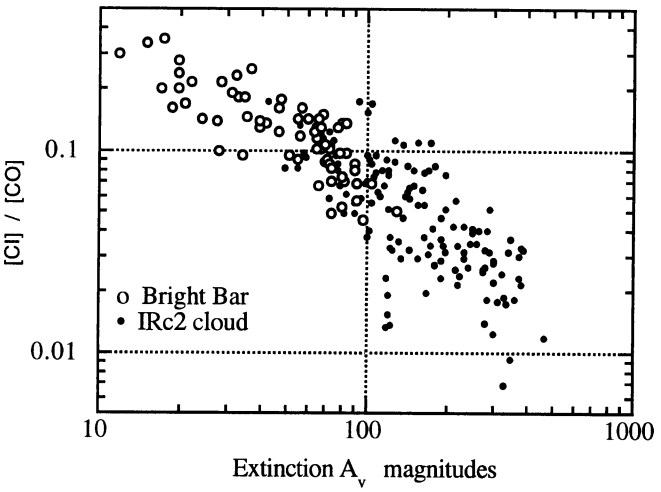

Fig. 13. Plot of the abundance ratio, [CI]/[CO] against the extinction. These values match well with the trend shown by Keene (1987) based on observations of a wide range of clouds observed with larger beams for the high A_v range, and from uv observations for $A_v < 1$ mag. The best fit power law gives a relationship $[CI]/[CO] \sim 3\ A_v^{-0.8}$, with a correlation coefficient of ~ 0.8. These data do not extend to lower A_v's shown in Fig. 6, since C I spectra were not taken at every point where ^{13}CO and $C^{18}O$ emission was detected

of [CI]/[CO] obtained from ultraviolet data towards a group of Orion stars by Federman et al. (1980), and others observed by Jenkins & Shaya (1979). This suggests that a close correlation between [CI]/[CO] and CO column densities extends over more than three orders of magnitude, covering the range $\sim 10^{16}$ - $5\ 10^{19}$ cm^{-2} (i.e. A_v values ~ 0.1 - 500), and $[CI]/[CO] \sim 10$ - 0.01.

The estimates of [CI]/[CO] shown in Fig. 13 cover the range of values typical of dense cloud cores and ionisation fronts (Keene 1987; White & Padman 1991), the highest values, which are predominantly towards the Bright Bar ionisation front, are at the upper end of the range predicted in recent chemical modelling for photodissociation regions (Pineau des Forêts et al. 1992; Schilke et al. 1993). Statistically there is no evidence that the C I column density systematically deviates from this power law relationship at the higher values of column density as originally suggested by Keene (1987), although it is true that the lowest value coincides with the 'hot core' position. The spread in the C I column densities is however large and further data sets similar to the present may be needed to address this problem further in a statistical manner.

The CO $J = 4 - 3$ emission towards the Bright Bar is clumpy, peaking close to the $J = 1 - 0$ ^{13}CO peaks in the map of Tauber et al. (1994), suggesting that the hot gas is emitted from the surface layers of dense clumps, rather than from the interclump medium, as predicted in the modelling of Meixner & Tielens (1993), and as observed towards M17 by White & Padman (1991). The $J = 1 - 0$ CO line is quite opaque across the whole Bar, since $T_{mb}\ (CO/^{13}CO)$ is typically 3 - 4 (White et al. 1995) with the NRO 15 arc second beam. Maps of the C I and CO $J = 4 - 3$ and $C^{18}O$ $J = 2 - 1$ distribution towards the Bright Bar are shown in Fig. 14.

The CO and C I emission regions are more intense about 15 arc seconds deeper into the molecular material in the ridge than at the positions of the highly excited gas at the edge of the ionisation front (shown by the narrow ridge seen in optical recombination lines (Münch & Taylor 1974), PAH molecules (traced by the 3.3 μm emission), and hot dust (traced by the 10 μm continuum radiation)). The lack of correlation between the PAH molecules, the H_2 or the 10 μm emission with either CO or C I suggests that a) ejected photoelectrons from the PAH molecules do not significantly heat the molecular or atomic gas as predicted by Verstraete et al. (1990), nor b) do the PAH molecules lead to a local increase of the abundances of carbon bearing molecules, which has been predicted as a consequence

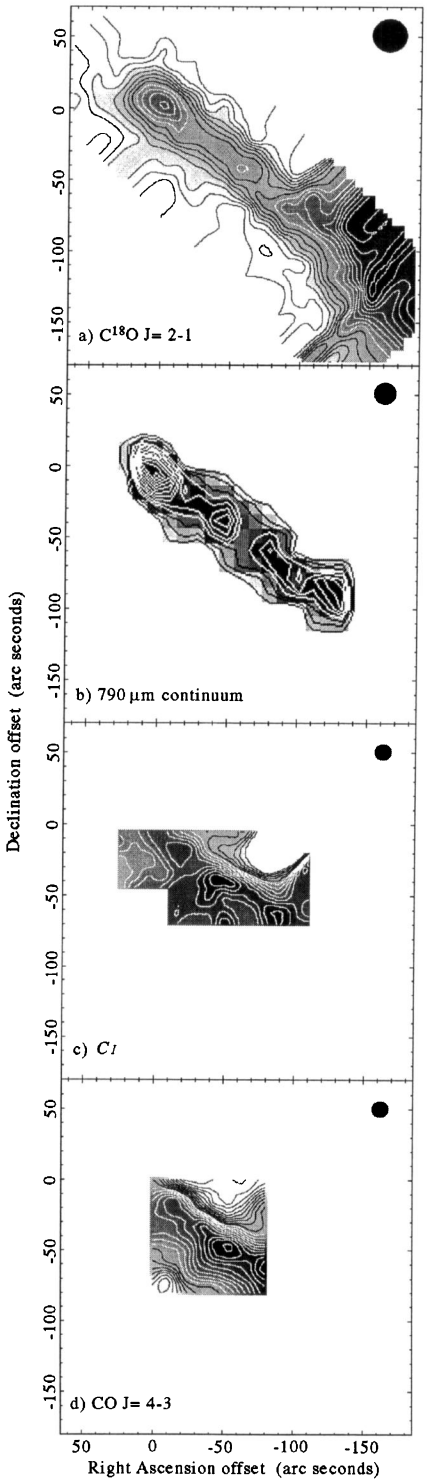

Fig. 14a–d. Maps of the integrated **a** $C^{18}O$ $J = 2 - 1$ lines over the velocity range 4 to 14 km s^{-1} with the first white contour at 3 K km s^{-1} with steps of 1.5 K km s^{-1} ,and the **b** 790 μm dust continuum (convolved to 10 arc second resolution) with contour levels linear in steps of 0.1 Jy / 10 arc second beam, compared with the **c** CO $J = 4 - 3$ with the first white contour level at 250 K km s^{-1} and intervals at 25 K km s^{-1} , and **d** C I lines with the first white contour level at 35 K km s^{-1} and intervals at 3 K km s^{-1} , towards the Bright Bar. The (0,0) position is the same as that of Fig. 4

of their high chemical reactivity (Lepp & Dalgarno 1988) - indeed the PAH's lie further into the HII region.

The Bright Bar is almost certainly heated both by shocks from the expanding HII region (White & Phillips 1988) and by ultraviolet radiation penetrating the clumpy gas. In the former case it is unlikely that a temperature enhancement would be observed, since post-shock radiative cooling would lead to a hot shock heated zone with a width less than $\sim$ 1 arc second wide (Phillips & White 1982; Omodaka et al. 1984). Graf et al. (1990) have also argued against the importance of shocks and dust-grain collisional heating as being the dominant excitation mechanism. A more likely source of heating for the gas in this bar is photoelectric heating (Tielens & Hollenbach 1985; van Dishoeck & Black 1988; Sternberg & Dalgarno 1989; Burton et al. 1990). These models have been successful at explaining the fine-structure line emission from photo-dissociation regions, but not the large column densities of hot gas present (Graf et al. 1993). They are however consistent with the fluorescent H_2 (Burton et al. 1990; Parmar et al. 1991) lines detected at some positions in the Bar. Tielens & Hollenbach (1985) have shown that the photoelectric effect is most efficient at $A_v \sim 3$ magnitudes; the column densities observed towards the centre of the Bar indicate $A_v \sim 50$ magnitudes, requiring that the Bar must be fairly clumpy for the ultraviolet radiation to penetrate.

Within the last few years the picture that has emerged to explain the unexpected high abundances of C I observed towards Galactic molecular clouds is a consequence of the photodissociation of CO molecules on the surfaces of dense clumps of gas by ultraviolet radiation. This apparently ubiquitous distribution of C I can then be understood in terms of time dependent chemistry on the surfaces of rotating molecular clumps (Monteiro 1991); the transfer of UV radiation scattered through a two-phase clumpy medium (Hobson & Padman 1993); or by multi-phase clumpy clouds (Meixner & Tielens 1993). Recent observational studies of C I have shown its abundance relative to CO; a) in shielded galactic molecular clouds (both cool and warm centred clouds) [C I]/[CO] $\sim$ 0.05 - 0.3 (Keene 1987; White & Padman 1991; Schilke et al. 1994); b) in molecular outflows [C I]/[CO] averages $\sim$ 0.2 (Walker et al. 1993; Minchin et al. 1994), c) in two external starburst galaxies (M82 and N253 by White et al. 1994b and Israel et al. 1994) [C I]/[CO] $\sim$ 0.3 - 0.5), c) in the J -shocked gas at the edge of the IC443 supernova remnant [C I]/[CO] $\sim$ 1 - 3 (White 1994), and d) in a Galactic high latitude translucent cloud [C I]/[CO] is $\sim$ 3 - 6 (Stark & van Dishoeck 1994). Finally, ultraviolet observations show that in low A_v material ($<$ 1 magnitude of optical extinction), [C I]/[CO] is in the range $\sim$ 1 - 50 (Federman et al. 1980; Frerking et al. 1989).

The [C I]/[CO] abundances in the Orion region can be compared to the predictions of photodissociation region models such as those of Hollenbach et al. (1991), Tarafdar (1991), Pineau des Forêts et al. (1992), Flower et al. (1994), Le Bourlot et al. (1993), Schilke et al. (1993, 1994). These models show that [C I] / [CO] can depend on the fractional ionisation of the gas. Whilst strong cosmic ray fluxes or shocks may be important to the high [C I]/[CO] abundances observed towards the starburst

galaxies and in IC443, they are less likely to be major contributors to the [CI]/[CO] ratio in more quiescent molecular cloud material such as the regions of the Orion Cloud away from IRc2. Flower et al. (1994) show that high [CI]/[CO] abundances can occur in a transition zone between high density gas, where the ion-neutral chemistry is driven by proton transfer with H_3^+ and lower density material where charge transfer with H^+ becomes more important. The largest CI column densities occur in gas with $n_H \sim 5500$ cm^{-3}, for a cosmic ray ionisation rate $\zeta = 10^{-17}$ s^{-1} (Pineau des Forêts et al. 1992).

These condition predicted in the modelling are very similar to those observed toward the Orion cloud. We still do not have good observational probes of the state of ionisation in photo dissociation regions, but even in the Bright Bar the [CI]/CO] ratios still fall in the ranges predicted by the modelling. It is possible to get high [CI]/CO] ratios anywhere outside this transition zone discussed by Flower et al. (1994), however the CO column densities may be lower as a consequence of the carbon being driven into CII. Schilke et al. (1994) model the CI abundances in the dark cloud TMC-1, getting good agreement with a photo dissociation region model even in relatively low density material ($n_{H2} \sim 2000$ cm^{-3} illuminated by the standard interstellar UV field and cosmic ray flux). The clearest example of CI excited in a photo dissociated gas is shown in Figs. 11 and 14, where the [CI]/[CO] ratio decreases sharply on moving deeper into the dense material in the bar, whilst remaining high just to the Northwest of the bar, in the direction of the ionising stars. This appears as a classic photo dissociation zone, clear stratification (progressing from the photo ionised side into the dense molecular ridge) being seen with the first layer being hot dust (3.3 and then 10 μm emission), then H_2, CI and finally CO.

5. Conclusions

a) The CI distribution is highly fragmented, and concentrated into several regions well separated from the IRc2 molecular core.

b) The CO $J = 4 - 3$ emission around IRc2 peaks along a narrow ridge lying to the South of the OMC1 core. The wings show a prominent bipolar outflow centred close to IRc2. Weak self-absorption is seen towards the 'Hot-core' source. The Bright Bar is seen clearly in the CO data, and has gas with brightness temperatures $\gtrsim 175$ K in places.

c) The CO column densities estimated from ^{13}CO data are about half those inferred from C^{18}O data. This highlights the dangers inherent in using ^{13}CO data alone to estimate cloud masses or column densities.

d) There is substantial isotopic fractionation of the ^{13}CO molecules, with N(^{13}CO)/N(C^{18}O) enhanced in the lower A_v regions of the cloud by $\sim$ one order of magnitude relative to the higher opacity parts of the OMC1 cloud. The ratio of column densities in the Orion Bright Bar scales as $\sim 90\, A_v^{-0.62}$, a trend that connects to lower A_v values inferred from ultraviolet data. There is no evidence for a similar trend for strong fractionation of C^{18}O or C^{17}O, although there may be a weak trend for the relative C^{18}O abundance to decrease in the lower A_v regions.

e) The average dust/gas mass ratio in the OMC1 cloud is ~ 0.025, for reasonable choices of dust properties. The values for the Bright Bar ionisation front are somewhat smaller. These values are however very uncertain due to lack of knowledge of the dust temperature and of β. The C^{18}O and C^{17}O line intensities are correlated with the continuum emission, suggesting that the isotopomeric CO lines are optically thin.

f) Comparison of the $^3P_2 - ^3P_1$ and $^3P_1 - ^3P_0$ CI lines suggests T_{ex} (CI) $\gtrsim 90$ K, which is close to T_{kin} derived from the CO $J = 2 - 1$ line of ~ 110 K.

g) The highest values of the [CI]/[CO] ratio are seen towards the northern section of the Orion molecular ridge, with a minimum just south of IRc2, close to the hot core. The abundance ratio [CI]/[CO] also shows a weak correlation with the CO $J = 2 - 1$ line temperature, and a strong correlation with the C^{18}O column density (which we suggest is to be proportional to the extinction), suggesting [CI]/[CO] $\propto 3\, A_v^{-0.8}$.

h) Clear evidence for stratification in the photo dissociation region of the Bright Bar is seen, with the CI lying adjacent to the CO peak, along the direction towards the exciting stars, but inside the H_2, 3.3 and 10 μm emission. The material associated with the Bright Bar shows the strongest ^{13}CO fractionation, and has the highest [CI]/[CO] abundance ratios, supporting models in which photo dissociation in the strong ultraviolet field at the edge of the Bar plays an important role in the gas excitation. In particular a strong decrease in the [CI]/[CO] abundance ratio is inferred between the material lying just outside the Bar, and in the denser gas further in, which is not yet fully illuminated by the external radiation field. The abundance ratios observed throughout the Orion Cloud and the Bright Bar are in good agreement with those predicted by photo dissociation chemical modelling.

Acknowledgements. We thank The UK Science & Engineering Research Council for supporting the Submillimetre Wave astronomy and instrumentation programme at QMW. The JCMT is operated by the Royal Observatory, Edinburgh on behalf of the UK Particle Physics and Astronomy Research Council, The Netherlands Organisation for Scientific Research and the Canadian National Research Council. We thank Juergen Stutzki and Peter Williams for commenting on an early draft of the mauscript, and helpful comments from the referee.

References

Anders, E. & Grevesse, N. 1989, Geochem. Cosmochim. Acta 53, 197.
Bachiller, T. and Cernicharo, J. 1986, A&A, 166, 283.
Becklin, E.E., Beckwith, S., Gatley, I. et al., 1976, ApJ, 207, 770.
Blake, G.A., Sutton, E.C., Masson, C.R. et al., 1987, 315, 621.
Burton, M.G., Geballe, T.R., Brand, P.W.J.L. et al., 1990, ApJ, 352, 625.
Burton, M.G., Moorhouse, A., Brand, P.W.J.L. et al., 1991, IAU Symposium 135, Interstellar Dust, ed. L.J. Allamandolla and A.G.G.M.Tielens, NASA Conference Publications CP-3036, p 87.
Castets, A., Duvert, G., Dutrey, A. et al. 1990, A&A, 234, 469.
Dickman, R.L. 1978, ApJ, Suppl, 37, 407.
Dutrey, A., Duvert, G., Castets, A. et al., 1993, A&A, 270, 468.
Ellison, B.N., Claude, S.X.M., Jones, A. et al., 1993, Digest International Conference on Mm and Submm Waves and applications.

Federman, S.R., Glassgold, A.E., Jenkins, E.B. et al., 1980, ApJ, 242, 545.
Flower, D.A., Le Bourlot, J., Pineau des Fôrets, G. et al., 1994, A&A, 282, 225.
Frerking, M.A., Langer, W.D. and Wilson, R.W. 1982, ApJ, 262, 590.
Frerking, M.A., Keene, J., Blake, G.A. et al., 1989, ApJ, 344, 311.
Fuente, A., Martin-Pintado, J., Cernicharo, J. et al., 1993, A&A, 276, 473.
Garay, G., Moran, J.M. and Reid, M. 1987, ApJ, 314, 535.
Gatley, I. & Kaifu, N. 1987 in Astrochemistry, ed M.S.Vardya & S.P. Tarafdar, D. Reidel Publishers, p 153.
Genzel, R., Harris, A.I., Jaffe, D.T. et al., 1988, ApJ. 332, 1049.
Genzel, R, 1991, NATO ASI 342, The Physics of Star Formation and Early Stellar Evolution, pp 155 - 219, editors Lada, C.J. and Kylafis, D.
Gierens, K.M., Stutzki, J. and Winnewisser, G. 1992, A&A, 259, 271.
Graf, U.U., Genzel, R., Harris, A.I. et al., 1990, ApJ (Letters), 358, L49.
Graf, U.U., Eckart, A., Genzel, R. et al., 1993, ApJ, 405, 249.
Greaves, J.S. and White, G.J. 1991, A&A Suppl, 91, 237.
Greaves, J.S. and White, G.J.: 1992, A&A, 259, 457.
Hayashi, M., Hasegawa, T., Gatley, I. et al., 1985, MNRAS, 215, 31p.
Hobson, M.P. and Padman, R. 1993, MNRAS, 264, 161.
Hobson, M.P., Padman, R., White, G.J. et al., 1994, A&A submitted.
Hollenbach, D.J., Takahashi, T. and Tielens, A.G.G.M. 1991, ApJ, 377, 192.
Howe et al. (1993), ApJ, 410, 179.
Israel. F.P., White, G.J. and Baas, F. 1994, A&A, in press.
Jaffe, D.T., Harris, A.I., Silber, M. et al., 1985, ApJ, 290, L59.
Jenkins, E.B. and Shaya, E.J. 1979, ApJ, 231, 55.
Keene, J., Hildebrand, R.H. and Whitcomb, S.E. 1982, ApJ, 252, L11.
Keene, J., Blake, G., Phillips, T.G. et al., 1986, ApJ., 299, 967.
Keene, J. 1987, in: Proceedings of SETI conference 'Carbon in the Galaxy: Studies from Earth and Space', NASA CP:3061.
Köster, B., Störzer, H., Stutzki, J. et al., 1994, A&A, 284, 545.
Lada, C.J., Lada, E.A., Clemens, D.P. et al., 1994, ApJ, 429, 694.
Le Bourlot, J., Pineau des Forêts, G., Roueff, E. et al., 1993, APJ, 416, L87.
Lepp, S. and Dalgarno, A. 1988, ApJ, 324, 553.
Martin, A.H.M. and Gull, S.F.: 1976, MNRAS, 175, 235.
Masson, C.R., Lo, K.Y., Phillips, T.G. et al., 1987, ApJ, 319, 446.
Meixner, M. and Tielens, A.G.G.M. 1993, ApJ, 405, 216.
Minchin, N., White, G.J. and Ward-Thompson, D. 1994, A&A, in press.
Monteiro, T.S. 1991, A&A, 241, L5.
Münch, G. and Taylor, K. 1974, ApJ, 192, L93.
Murata, Y., 1992, PhD Thesis, University of Tokyo.
Omodaka, T., Hayashi, M.,Hasegawa, T. 1984, ApJ, 282, L77.
Omodaka, T., Hayashi, M., Hasegawa, T. et al., 1994, Preprint.
Parmar, P.S., Lacy, J.H. and Achtermann, J.M. 1991, ApJ, 372, L25.
Penzias, A.A. 1981, ApJ, 249, 518.
Phillips, J.P. and White, G.J. 1982, MNRAS, 199, 1033.
Pineau des Forêts, G., Roueff, E. and Flower, D. 1992, MNRAS, 258, 45p.
Richer, J.S. 1992, MNRAS, 245, 24p.
Schilke, P., Carlstrom, J.E., Keene, J. and Phillips, T.G. 1993, ApJ, 417, L67.
Schilke, P., Keene, J., Le Bourlot, J. et al., 1994, preprint.
Sutton, E., Blake, G., Masson, C. et al., 1985, ApJ, 315, 621.
Stark, R. and van Dishoeck, E.F. 1994, A&A, 286, 443.
Sternberg, A. and Dalgarno, A. 1989, ApJ, 338, 197.
Tarafdar, S.P. 1991, MNRAS, 252, 55p.
Tauber, J.A., Tielens, A.G.G.M., Meixner, M. et al., 1994, ApJ, 422, 136.
Tielens, A.G.M and Hollenbach, D. 1985, ApJ, 291, 722
Turner, B.E., Xu, L. and Rickard, B.J. 1992, ApJ, 391, 158.
Turner, B.E. 1993, ApJ, 405, 229.
van Dishoeck, E., and Black, J. 1988, ApJ., 334, 771.
Verstraete, L., Léger, A., d'Hendecourt, L. et al., 1990, A&A, 237, 436.
Walker, C.K., Narayanan, G., Büttgenbach, T.H. et al., 1993, ApJ, 415, 672.
Werner, M.W., Gatley, I., Harper, D.A. et al., 1976, ApJ, 204, 420.
Werner, M.W., Crawford, M.K., Genzel, R. et al., 1984, ApJ, 282, L81.
White, G.J. and Phillips, J.P. 1988, A&A, 197, 253.
White, G.J. and Padman, R. 1991, Nature, 354, 511.
White, G.J., Ellison, B., Claude, S.X.M. et al., 1994, A&A, 284, L23.
White, G.J. 1994, A&A, 283, L25.
White, G.J., Greaves, J.S., Hasegawa, T. et al., 1995, in preparation
White, G.J., Casali, M.M. and Eiroa, C. 1995, in press A&A.
Wilson, T.L., Serabyn, E., Henkel, C. et al., 1986, A&A, 158, L1.
Wright, M., Sandell, G., Willner, D.J. et al., 1992, ApJ, 393, 225.
Young, J., Goldsmith, P.F., Langer, W.D. et al., 1982, ApJ, 261, 513.
Yusef-Zadeh, F. 1990, ApJ, 361, L19.
Zmuidzinas, J., Betz, A.L. Boreiko, R.T. et al., 1988, ApJ, 335, 774.

This article was processed by the author using Springer-Verlag LaTeX A&A style file version 3.